Schlieren Imaging of Single-Fin Missile models in a De-Laval Nozzle Test Section

Nayhel SHARMA*,[1], Bharat Ankur DOGRA[2], Rakesh KUMAR[1]

*Corresponding author
[1]Aerospace Engineering Department,
Punjab Engineering College (Deemed to be University),
Chandigarh, India,
nayhel.sharma@gmail.com
[2]SOB-CCE, University of Petroleum and Energy Studies,
Dehradun, India

DOI: 10.13111/2066-8201.2021.13.2.14

Received: 03 October 2020/ Accepted: 03 February 2021/ Published: June 2021

Abstract: *The experimental study (Schlieren photography) to characterize the flow behavior around a semi-cylindrical missile model having a single planar and wrap-around fin surface is performed inside a modified De-Laval nozzle test section capable of sustaining an airflow at Mach number ~1.7M. The images obtained from this schlieren technique is compared with flow field contour images of the similar missile models at similar flow conditions. The experiments are performed on a modified two-walled glassed section to assist the Schlieren imaging. The test section is calibrated preliminary to the experiments to assure the supersonic fluid flow. A comparison of flow images around the two types of fins further helps in characterizing the flow in their vicinity.*

Key Words: *Schlieren Photography, Aerodynamics, Missile, Planar and Wrap-around Fins*

1. INTRODUCTION

Flow visualizations were experimentally investigated on two contrasting single-fin missile models using Schlieren Photography. The experiments were performed on a planar fin, and a wrap-around fin surface mounted vertically over a scaled-down semi-cylindrical missile model, which was computationally studied [1], [2]. The geometry and the dimensions of the single fin missile models were adapted from the computational studies of Sharma [1]–[4] et al., which were based only upon single wrap-around fin missile model, experimental and numerical studies of Tilman [5]–[9], et al. The scaled-down single fin missile models resolved the limitations of a small test section and also aided in the comprehension of fluid flow in the vicinity of the fin surface.

An existing supersonic open jet wind tunnel apparatus was augmented with a De-Laval test section. The A De-Laval nozzle test section was fabricated based upon the design study of Khurana [10] et al. Theoretically, this De-Laval nozzle test section was designed for Mach number ~2.0M. The test section was calibrated and verified for true Mach number, which was lesser than the predicted flow speed (~1.7M). Establishing the true value of the Mach number inside the test section, the Schlieren imaging setup erected, and the experiments were carried out on a single planar fin and a wrap-around fin missile model.

Subsequently, computational studies were performed upon the single fin missile models kept in a computational domain, unlike the wind tunnel, at similar flow conditions, i.e., relative to Mach number ~1.7M. The flow visualizations obtained from these computational studies, consisting of static pressure contours, were simultaneously compared with the images obtained from the Schlieren photography of the missile models inside the test section. The main objectives of this study were to:

1. Fabricate and calibrate a De-Laval nozzle test section for supersonic flow.
2. Perform schlieren photography for a single planar fin missile model and compare the image results with the flow visualizations obtained from its computational counterpart.
3. Perform schlieren photography for a single wrap-around fin missile model and compare the image results with the flow visualizations obtained from its computational counterpart.

2. EXPERIMENTAL SETUP

De-Laval Nozzle. The nozzle test section was fabricated based upon the supersonic Nozzle design [10]. The Code mentioned in Reference [10] was executed for Mach number ~2M, from where coordinates of the upper part convergent-divergent contour of the nozzle were obtained [11], [12]. These coordinates were then transferred to Solid works® to generate the solid contour of the nozzle. The test section was added at the end of the expansion region. The designed nozzle was augmented on an open jet supersonic wind tunnel capable of producing a Mach number ~4.0M for approximately 240secs in the Aerodynamics Laboratory, Aerospace Engineering Department of Punjab Engineering College (Deemed to be University), Chandigarh, India. A circle to the square adapter is designed to convert the circular cross section of settling chamber to the nozzle inlet square cross section. (Figure 1) The result of this CAD model is the combination of two parts:

1. Circle to Square Adapter
2. Nozzle Contour

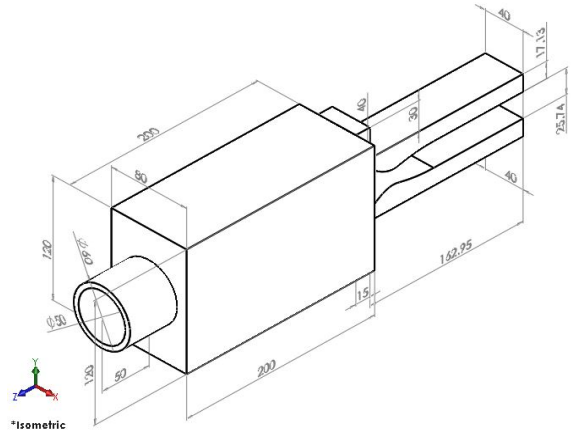

Figure 1: Isometric View of the block and the nozzle. (Dimensions in mm) [10]

Weight Reduction, drilling holes for holding the glass mirror, and excess material removal were performed at Machine Shop, Production Engineering Department of Punjab Engineering College (Deemed to be University), Chandigarh, India (Figure 2). An industrial silicon sealant was applied on the edges between the test section and the mirror to prevent any air leakage through the test section.

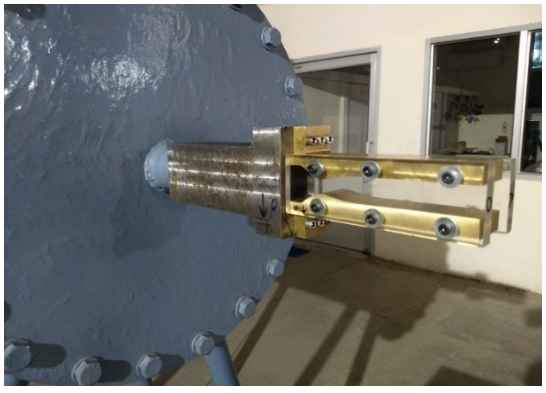

Figure 2: Complete De-Laval Nozzle with side mirrors on the test Section

Single Fin Missile Model. Manufacturing of the experimental scaled-down models was carried out for a planar and a WAF single fin model (Figure 3). The models were sized for maximum data reduction (resolution) while avoiding wind-tunnel blockage. The single planar fin model's projected area was 2.43% of the wind tunnel's cross-sectional area in the flow direction. Similarly, the single fin WAF model's projected area was 2.77% of the wind tunnel's cross-sectional area in the direction of the flow (Less than 3%). Also, considering the missile body model as a semi-cylinder and adding its projected area in the direction of flow, the the designed assembly remains below 10% in terms of blocking [13]–[18]. In the case of the planar missile model, the projected area was 6.2%, and for the wrap-around fin model, the projected area was 6.54% of the total cross-sectional area of the test section. Initially, the single fin missile models were 3D printed. However, the 3D printed models lacked in strength and failed during the experimentation (Figure 4). The machined missile models' dimensions were scaled to 1:2 of their computational counterparts, Sharma [1]–[4] et al.

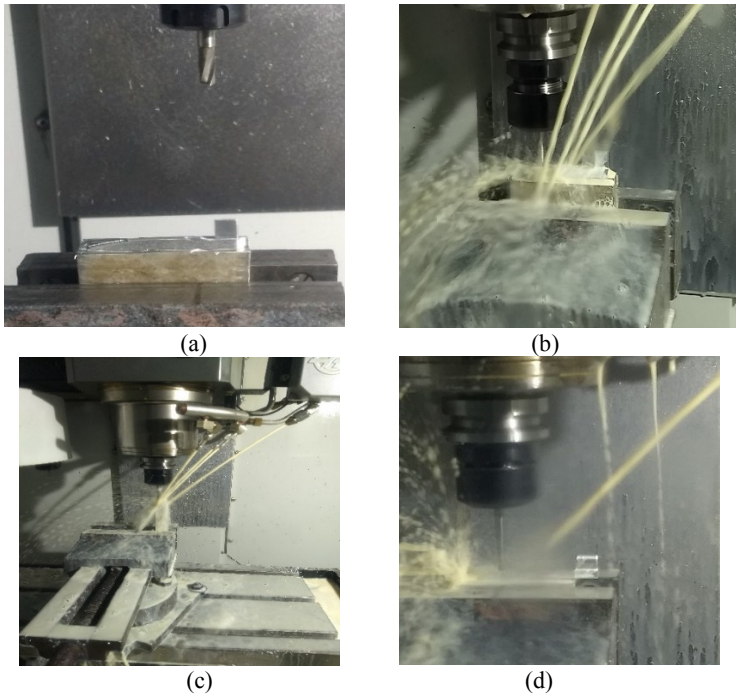

(a) (b)

(c) (d)

Figure 3: (a)-(d) CNC machining of misile models. (alluminium)

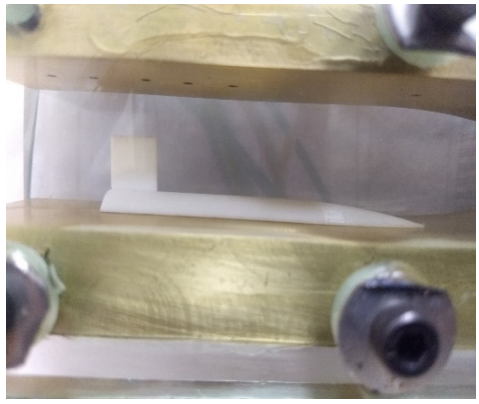

Figure 4: (Failed) 3D printed missile model placed in the test section

Instrumentation and Schlieren Photography Setup. The Schlieren Images were recorded digitally using a Nikon® D5100, digital single-lens reflex camera.

The color of the light was bright yellow, emitted from a halogen light source (1000W, 220V) with a control unit, a lens with setting arrangement & proper air cooling with proper holding stand (Tripod).

This light source had a Knife-edge(s) with adjustable X & Y axes. Along with that, the apparatus consisted of two high-quality parabolic mirrors having a diameter of 8 inches, with a holding of a square disc, each mounted on a tripod.

The parabolic mirrors had a front coating of aluminum, the surface finish of lambda 4, and a focus of 1.5 meters (approximately). The complete installation and setup of the apparatus has been shown in (Figure 5).

Calibration of the De Laval Test Section. The affirmation of supersonic flow was done by carrying out Schlieren photography of different geometry heads and by observing the shock formations ahead of these probes (Figure 6).

Using the Compressible flow pitot tube equation (Supersonic), a pitot probe in a supersonic stream would have a bow shock ahead of it.

This complicates the flow measurement since the bow shock will cause a drop in the total pressure, from $p_{\circ 1}$ to $p_{\circ 2}$, the latter being sensed by the pitot port.

It's useful to note that the shock will also cause a drop-in density $\rho_{\circ}$, but, $h_{\circ}$ will not change.

The pressures and Mach number immediately behind the shock are related by:

$$\frac{p_{\circ 2}}{p_2} = \left(1 + \frac{\gamma - 1}{2} M_2^2\right)^{\gamma/\gamma - 1}$$

Twenty observations were recorded for the calculation of Mach number (M_2). Based on the mean (SEM) standard error with a confidence level of 95%, the value for static pressure and the stagnation/ total pressures were 0.9401Bar & 1.2456 Bar. $M_2 = 0.6398M \pm 0.0027$. Henceforth, we use equation [19]:

$$M_2^2 = \frac{(\gamma - 1)M^2 + 2}{2\gamma M_1^2 - (\gamma - 1)}$$

Hence, the theoretical value of the supersonic Mach number (M_2) in the test section was confirmed as $M_2 = 1.70M \pm 0.0027$.

Figure 5: Schlieren Photography Setup

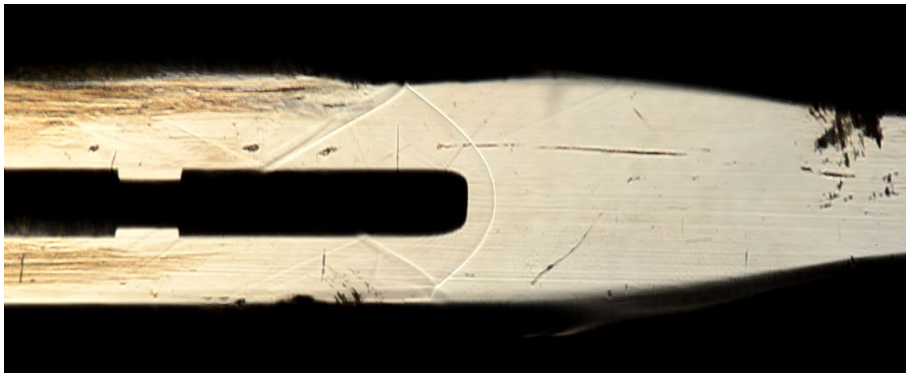

Figure 6: Bow Shock formation ahead of the blunt-edged probe.

The true run time of fully developed steady supersonic flow was calculated ~30secs approximately. Finally, the installation of the nozzle, its calibration, and experiments (Schlieren photography) [20] were carried out at Aerodynamics Laboratory, Aerospace Engineering Department of Punjab Engineering College (Deemed to be University), Chandigarh, India.

Figure 7: Missile model in the test section

Computational Setup. In the current study, numerical simulations were performed using the FLUENT® module, a trademark of ANSYS® [21]. In the current numerical study the density-based approach was used due to the participation of high-speed compressible flow with time steady absolute velocity formulation and was adopted from the CFD review papers [22], [23]. The governing equations employed five non-linear, differential, and coupled three-dimensional equations consisting of a set of the continuity equation, three momentum equations, and one energy conservation equation. These equations are collectively called the Navier-Stokes equations (NS), and these are mentioned below:

Continuity equation:

$$\partial\rho/\partial t + \nabla.(\rho V) = 0 \quad (1)$$

Momentum equation:

$$\rho\,\partial V/\partial t = \nabla.\tau_{ij} - \nabla p + \rho F \quad (2)$$

Energy equation:

$$\rho\,\partial e/\partial t + \rho(\nabla.V) = \partial Q/\partial t - \nabla.q + \Phi \quad (3)$$

The details of the computational counterpart have been presented in Table 1.

Table 1: Computational boundary conditions in accordance with the test Section

Freestream Velocity Corresponding to Mach Number 1.7 in (m/s)	Air Density	Temperature (Kelvin)	Pressure (Pascal)	Boundary Conditions at the Inlet, Outlet & Far-field	Missile and Fin Body
578.2782 m/s	*Ideal Gas – 1.22 kg/m³*	*288.15K*	*101325Pa*	*Pressure far-field conditions*	*No-slip wall Condition*

3. EXPERIMENTAL AND COMPUTATIONAL RESULTS OF SINGLE-FIN PLANAR MODEL

In order to obtain the initial understanding of the flow field ahead of the fin, full model imaging was performed with the planar fin model in the test section.

The series of images consists of *(i)* the image of the model in the test section in no flow condition, (Figure 8) *(ii)* the image of the model in the test section inflow condition and the first shockwave approaching, (Figure 9) *(iii)* the image of the complete model which is fully developed supersonic flow with observable shock formation at the nose of the missile body and ahead of the fin structure, (Figure 10) *(iv)* the image of the model in the test section which is fully stable supersonic flow with a focus on the fin structure (Figure 11).

Figure 8: Test section with planar fin missile model imaging in a no-flow condition

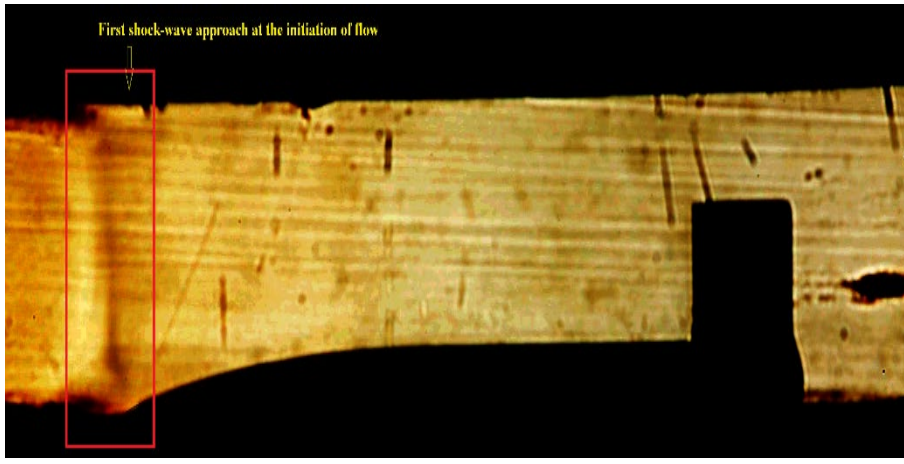

Figure 9: Formation of shockwave at the initiation of flow

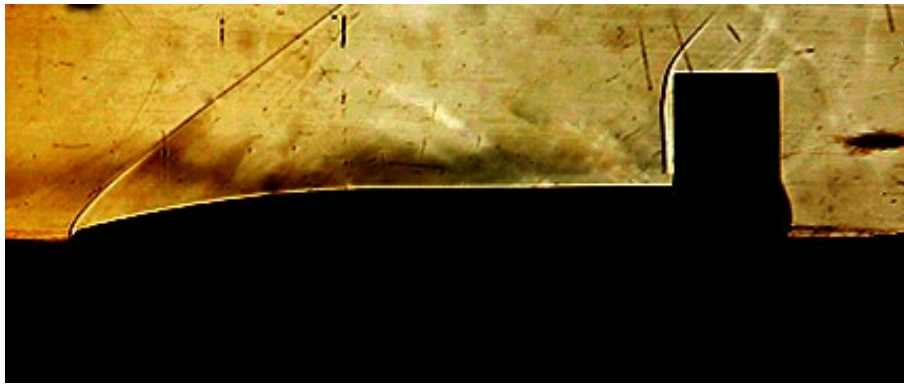

Figure 10: Shockwave pattern formation in the fully developed supersonic flow

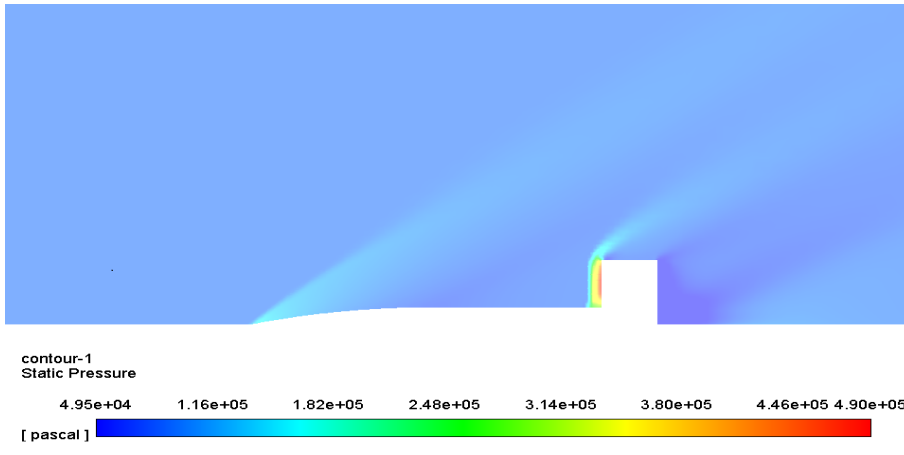

Figure 11: Static Pressure contours over planar missile model at Mach 1.7M.

In both images (Schlieren & computational) (Figure 8 to Figure 11), it may be noted that the bow shock remains detached over the full height of the fin at Mach 1.7M. The shocks originating from the missile body's nose can be seen reflecting off of the opposing wind tunnel wall, just above the fin. (Deliberately made out of focus to identify model's flow behavior)

Along with that, the other shock patterns/structures/ disturbances in the image (made out of focus) were caused by small imperfections in the test section wall associated with the holes made for static pressure measurements. The boundary layer over the model is visible.

Figure 12 and Figure 13 are the images produced by Schlieren and computations, which have been enlarged to show the details of the flow structures in front of the fin-body juncture. The shock-boundary layer interaction produces the same type of λ-shock typically observed in front of the blunt fins [24]–[30]. A stagnation point can be observed at the parting line in the flow field of the planar blunt fin.

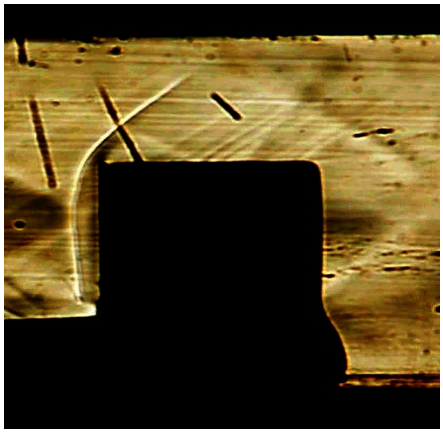

Figure 12: Shockwave formation ahead of the fin

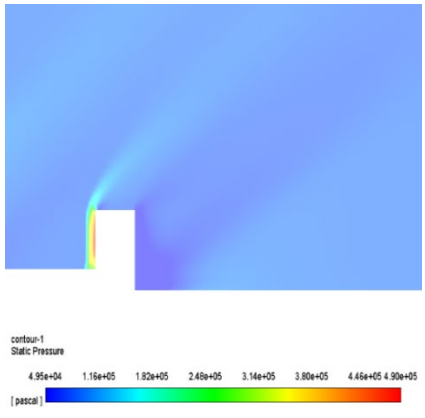

Figure 13: Static Pressure contours ahead of the planar fin at Mach 1.7M

4. EXPERIMENTAL AND COMPUTATIONAL RESULTS OF SINGLE-FIN WRAP-AROUND FIN MODEL

Subsequently, Schlieren imaging was performed for the WAF model in the test section. In this case, the imaging was done from both the concave and convex side of the fin. Figure 14 shows the missile model in no-flow conditions. The Schlieren images from the concave side of the fin are presented in Figure 15 and the static pressure contours from the computational analysis are shown in Figure 16, for comparison. As can be seen in the computational image, the concave side of the fin behaves like a converging nozzle and the leading edge on the concave side of the fin forms a weak shock ahead of the fin structure up to the mid chord of the fin. The reflected shock waves from the test section walls and the shockwaves originating from the test section's imperfections have been made out of focus.

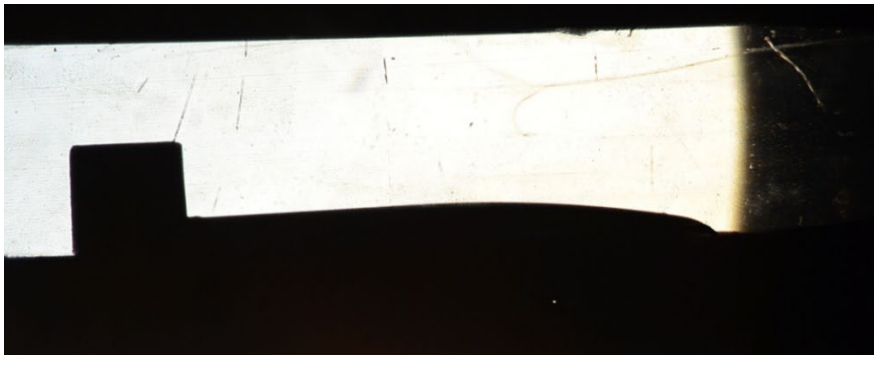

Figure 14: Test section with wrap-around fin model, Schlieren imaging in no-flow condition

Figure 15: Test section with the model, Schlieren image from the concave side of the fin

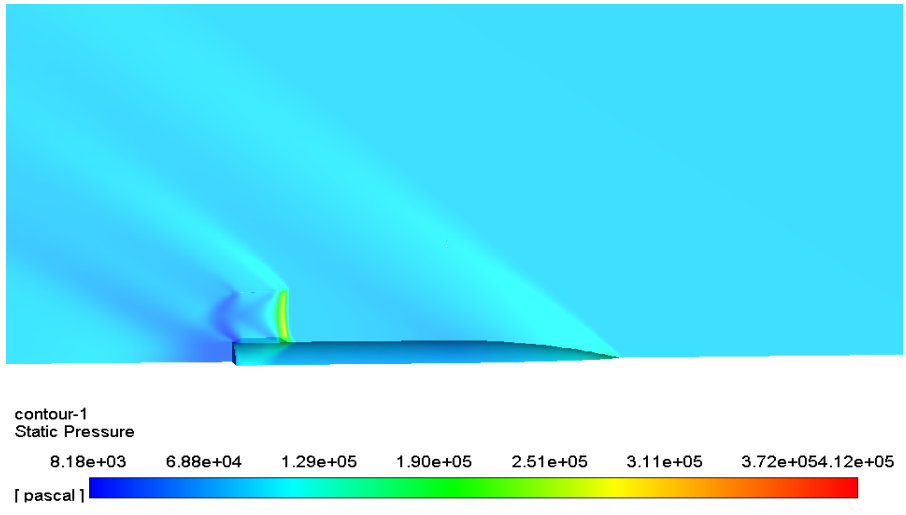

Figure 16: Static Pressure contours over wrap-around fin missile model (Concave side) at Mach 1.7M

Closely examining the WAF, it can be observed that the shock wave forms much ahead of the fin leading edge when compared to the Planar fin. The shock-boundary layer interaction produces the same type of λ-shock typically observed in front of the blunt fins. However, it may be attributed to the interaction of reflected shocks from the test section wall. The curved fin's top leading edge behaves like a blunt object, resulting in bow-shock formation much ahead of the fin tip (Figure 17 and Figure 18).

Figure 17: Shockwave formation as observed from the concave side of the fin (Schlieren)

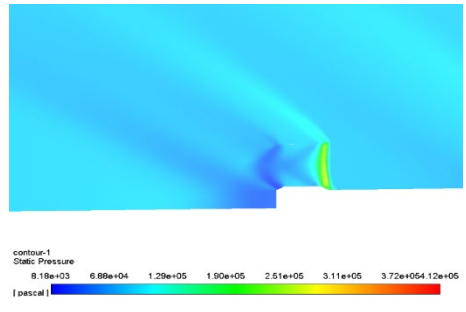

Figure 18: Static Pressure contours ahead of the concave side of the fin, (wrap-around) at Mach 1.7M

The Schlieren images from the convex side of the fin are presented in Figure 19 and the static pressure contours from the computational analysis is shown in Figure 20, for comparison.

As can be seen from the static pressure contours, the leading edge of the fin experiences extreme pressure increase and the presence of λ-shock at the missile-fin juncture. Closely observing the Schlieren image, the presumption that the shock disturbance at the fin- missile juncture may result from interactions due to reflected shock waves from the test section walls may not completely be the sole reason for this phenomenon. It may be assumed that the root of the fin, on the fin's convex side, may behave as a blunt fin, which may be the cause of asymmetry of the flow on either side of the fins.

Closely looking at the images focused on the fin (Convex side), the shock wave's attachment can be observed at the fin's top leading edge.

The fin's convex side experiences a great increase of pressure forces at the full length of the fin's leading edge.

This attachment of flow may be caused by the expansion of flow on the convex side of the fin (Figure 21 and Figure 22*)*.

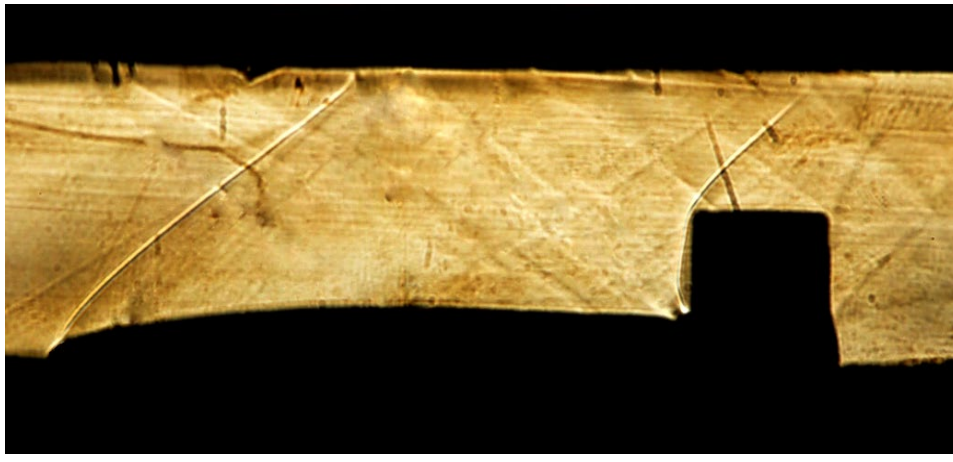

Figure 19: Test section with the model, Schlieren image from the convex side of the fin

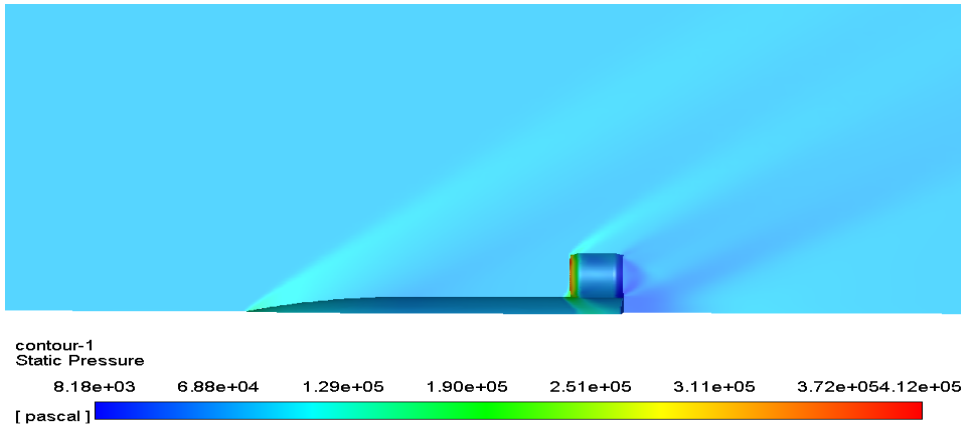

Figure 20: Static Pressure contours over TW02 (Convex side) at Mach 1.7M

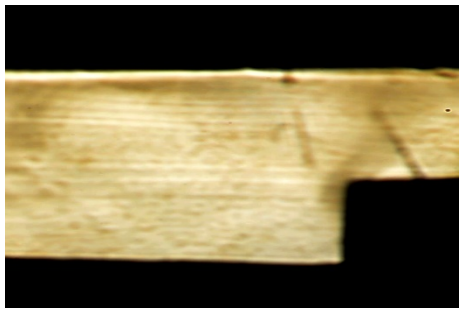

Figure 21: Shockwave formation as observed from the convex side of the fin (Schlieren)

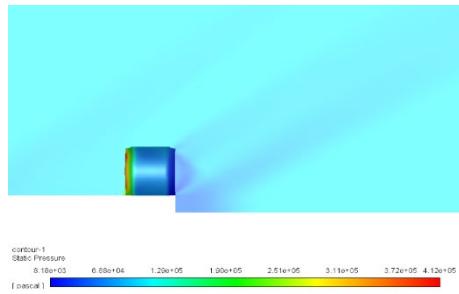

Figure 22: Static Pressure contours ahead of the convex side of the fin, (wrap-around fin) at Mach 1.7M

5. CONCLUSIONS

The Schlieren imaging of both the planar missile model and the wrap-around fin missile model was successfully captured. The flow inside the test section seemed to be steady to record the shock images with little or no disturbances. The same can be reasonably compared with computational counterparts. The Mach number ~1.7M computations gave favourable results in terms of depicting the shock formation. This experimentation helped in understanding the flow physics around the fins as well as the complete model. The shock formations originating from the body's nose may have little effect on the flow-field around the fin structure (If reflected shock waves are to be considered and the shocks originating from the imperfections in the test section). The planar blunt fin exhibited an identical flow phenomenon as that of a flat plate. It can be noted that the shock along the full height of the planar fin remains the same except at the fin missile juncture. Also, the boundary layer over the missile and fin wall surface is easily identifiable. In the case of the wrap-around fin model, both the concave and convex sides of the fins show different shock structures. In the case of the fin's concave side, the fin's top leading edge behaves like a blunt surface, whereas in the case of the convex side of the fin, the fin's bottom edge (missile fin juncture) behaves as a blunt surface in the flow field. The shock layer is detached significantly on the leading edge of the fin's concave side, whereas the shock layer is absent on the convex side of the fin's leading edge. The latter phenomenon may be attributed to the expansion of waves on the convex side of the fin. This attachment may cause an extreme rise of pressure on the fin's leading edge on the convex side, which is prominent in the images from the computations. Thus, this small-scale experimental analysis can be used as a visual validator for the computational counterpart, which has a flow at Mach 1.7M. These experiments' inferences may help the designer modify the fin geometry for favorable aerodynamic results, especially in the leading-edge variations.

REFERENCES

[1] N. Sharma, P. Saini, H. Chaudhary, G. Nagi, and R. Kumar, Comparison of Flow field in the proximity of A Single Planar & Wrap-around Fin, *Int. J. Aviat. Aeronaut. Aerosp.*, vol. **6**, no. 4, p. 31, 2019.

[2] N. Sharma and R. Kumar, Investigation of flow - field around a single generic planar fin using CFD, *SN Appl. Sci.*, vol. **2**:63, no. January 2020, p. 12, 2020.

[3] N. Sharma and R. Kumar, The simulation of single wrap-around fin on a semi-cylindrical missile body, *Aircr. Eng. Aerosp. Technol.*, vol. **92**, no. 3, pp. 418–427, Jan. 2020.

[4] N. Sharma, G. S. Nagi, H. Chaudhary, P. Saini, and R. Kumar, Computational Flow Field Analysis around a Single Wrap-around Fin, *INCAS Bull.*, vol. **12**, no. 2, pp. 199–216, https://doi.org/10.13111/2066-8201.2020.12.2.17, Jun. 2020.

[5] J. R. Huffman, C. P. Tilmann, T. A. Buter, and R. D. W. Bowersox, *Experimental Investigation of the Flow Structure in the Vicinity of a Single Wrap-Around Fin at Mach 2.9*, 1996.
[6] R. D. W. Tilmann, C. P. Huffman, Jr R. Buter, T. A. Bowersox, Experimental Investigation of the Flow Structure Near a Single Wrap-around Fin, vol. **34**, no. 6, 1997.
[7] C. P. Tilmann, J. R. Huffman, T. A. Buter, and R. D. W. Bowersox, Characterization of the flow structure in the vicinity of a wrap-around fin at supersonic speeds, *Instrumentation*, no. January, 1996.
[8] C. P. Tilmann, T. A. Buter, and R. D. W. Bowersox, Characterization of the Flow field near a Wrap-Around Fin at Mach 2.8, *J. Aircr.*, vol. **35**, no. 6, pp. 868–875, 1998.
[9] C. P. Tilmann, Numerical and Experimental Investigation of the Flowfield Near a Wrap-Around Fin, 1997.
[10] P. Khurana, J. Saurabh, H. Chaudhary, G. Singh, K. Singh, and T. Siag, Supersonic Nozzle Design using method of characteristics, in *International Conference on Theoretical, Applied, Computational and Experimental Mechanics*, 2017, pp. 1–8.
[11] D. R. Zucker and O. Biblarz, *Fundamentals of Gas Dynamics*, Second. Monterey, California: John Wiley & Sons, INC, 2002.
[12] J. D. Anderson, *Modern compressible flow: with historical perspective*, Second., vol. **12**. McGraw-Hill New York, 1990.
[13] K. Takeda and M. Kato, Wind tunnel blockage effects on drag coefficients and wind-induced vibrations, *Japanese Soc. Biofeedback Res.*, vol. **19**, pp. 709–715, 1992.
[14] E. C. Maskell, A Theory of the Blockage Effects on, Bluff Bodies and Stalled Wings in a Closed Wind Tunnel, *Reports Memo.*, no. **3400**, 1963.
[15] S. Perzon, On blockage effects in wind tunnels - A CFD study, *SAE Tech. Pap.*, no. 724, 2001.
[16] J. E. Hackett and K. R. Cooper, Extensions to Maskell's theory for blockage effects on bluff bodies in a closed wind tunnel, *Aeronaut. J.*, vol. **105**, no. 1041–1050, pp. 409–418, 2001.
[17] C. K. Choi and D. K. Kwon, Wind tunnel blockage effects on aerodynamic behavior of bluff body, *Wind Struct. An Int. J.*, vol. **1**, no. 4, pp. 351–364, 1998.
[18] T. Y. Chen and L. R. Liou, Blockage corrections in wind tunnel tests of small horizontal-axis wind turbines, *Exp. Therm. Fluid Sci.*, vol. **35**, no. 3, pp. 565–569, 2011.
[19] J. D. Anderson, *Fundamental of Aerodynamics*, Fifth. New York, 2010.
[20] T. P. Davies, Schlieren photography - short bibliography and review, pp. 37–42, 1981.
[21] * * * ANSYS Inc., ANSYS FLUENT 12.0 Theory Guide, *Release 12.0 © ANSYS, Inc.*, 2009. [Online]. Available: https://www.afs.enea.it/project/neptunius/docs/fluent/html/th/main_pre.htm.
[22] N. Sharma and R. Kumar, Missile Grid Fins Analysis using Computational Fluid Dynamics: A Systematic Review, *Incas Bull.*, vol. **11**, no. 1, pp. 151–169, https://doi.org/10.13111/2066-8201.2019.11.1.12, 2019.
[23] N. Sharma and R. Kumar, A Ready Reckoner of CFD for Wrap-around Fins, *INCAS Bull.*, vol. **11**, no. 2, pp. 155–170, https://doi.org/10.13111/2066-8201.2019.11.2.13, Jun. 2019.
[24] D. S. Dolling and S. M. Bogdonofft, Blunt Fin-Induced Shock Wave / Turbulent Boundary-layer Interaction, *AIAA J.*, vol. **20**, no. 12, pp. 1674–1680.
[25] L. G. Kaufman II, R. H. Korkegi, and L. C. Morton, Shock Impingement Caused by Boundary Layer Seapration Ahead of Blunt Fins, *11th AIAA Aerosp. Sci. Meet.*, vol. **10**, no. 12, pp. 1363–1364, 1973.
[26] C. M. Hung and P. G. Buning, Simulation of blunt-fin-induced shockwave and turbulent boundary-layer interaction, *J. Fluid Mech.*, vol. **154**, pp. 163–185, 1985.
[27] R. Sedney and C. W. Kitchens, Separation ahead of Protuberances in Supersonic Turbulent Boundary Layers, *AIAA J.*, vol. **15**, no. 4, pp. 546–552, 1977.
[28] D. Settles, G. S. Dolling, Experimental Research on Swept Shock Wave Boundary Layer Interactions, no. April, 1986.
[29] B. Edney, *Anomalous Heat Transfer and Pressure Distributions on Blunt Bodies at Hypersonic Speeds in The Presence of An Impinging Shock*, 1968.
[30] S. Hiers and W. J. Lozlbsky, *Effects of Shockwave Impingement on the Heat Transfer on a Cylindrical Leading Edge*, 1967.